ACTA SCIENTIFIC MICROBIOLOGY

Volume 2 Issue 9 September 2019

Research Article

Impacts of the Extreme Conditons of Environments on RNA's structure and function from the *Avocado Sunblotch* Viroid : Applicaton of NIR-Raman Spectroscopy and ad hoc Baro-Bio-Reactor

Gaston Hui Bon Hoa[1]*, Sergei G. Kruglik[2] and Marie-Christine Maurel[3]

[1]*National Institute of Health and Medical Research, INSERM, France*

[2]*Sorbonne Université, CNRS - Institut de Biologie Paris-Seine, Laboratoire Jean-Perrin, F-75005, Paris*

[3]*ISYE4B – UMR 7205, 7505 Paris - UPMC University in Paris, Laboratoire ANBioPhys, France*

***Corresponding Author:** Gaston Hui Bon Hoa, National Institute of Health and Medical Research, INSERM, France.

Received: August 06, 2019; **Published:** August 30, 2019

DOI: 10.31080/ASMI.2019.02.0358

Abstract

The typical environment for biomolecules *in vivo* is highly crowded. Molecular crowding effects can affect radically RNA folding mechanism as well as stability and function. To mimic in dilute solution, some of these effects, a combination of biophysical techniques and extreme physical-chemical parameters changes is used to probe the structural flexibility and function of RNA from *Avocado Sunblotch* viroids. Such viroids are non encapsidated RNA plant pathogens which possess a catalytic hammerhead ribozyme activity. To date, little is known regarding the conformation of ribonucleic acids (RNA), and the ways by which such viroid induces diseases. NIR Raman spectroscopy study gives several markers which are sensitive to RNA folding and structural changes. A typical « A-type » RNA conformation with ordered double helical content and a C3'-endo/anti sugar pucker configuration are found which are destabilized by high temperature. Deuteration not only decreases RNA self-cleavage activity but induces a new secondary structure. Surprisingly, the self-cleaved RNA Raman vibrational modes, exhibit noticeable frequency downshifts suggesting that phosphodiester and phosphodioxy structures are modified. A designed baro bio-reactor has been developped which allows at constant pressure, rapid injection of activators and sampling out of products. Bell-shape temperature-profiles of RNA's cleavage activity are obtained which is independent of the pressure. However pressure decreases the rates in a non-linear manner with an initial activation volume $\Delta V\ddagger = +20.5$ ml/mole, and an activation isothermal compressibility $\Delta\beta\ddagger = 8\ 10^{-6}\ MPa^{-1}$ suggesting that the active site is controlled by complex multi-conformers. However, study on a model full-length ribozyme (54), shows clearly two distinct pressure-sensitive activities indicating the participation of a fast cleaving and a slow cleaving conformers.

Keywords: Environment; Biomolecules; Structures; *Avocado Sunblotch*

Introduction

Typical environment for biomolecules *in vivo,* is highly crowded due to the presence of various macromolecules in the cell, typically in the range of 300-400 mg/ml [1] corresponding to 20-30% macromolecular fraction [2,3]. In such conditions, subtle conformational transition, binding and activity may be affected by « molecular crowding » effects such as volume exclusion which is suggested to favor compact conformations based on entropic arguments [4,5] as well as hydration of nucleic acids [6,7]. Repulsive electrostatic interactions and mechanical environmental stress [8,9] similarly induce compaction and/or destabilization of the structure of nucleic acids. Biophysical properties of biomolecules inside cells can be expected to be quite different from those measured in dilute solutions. To mimic the cellular crowding effects in dilute solutions, two perturbation biophysical techniques are developed such as NIR Raman Spectroscopy which is an excellent tool to characterize the RNA's structures and conformations, in response to changes in extreme physico-chemical parameters and a high pressure bio-reactor permitting injection of activators and sampling out of products in order to probe self-cleavage activity of ASBVd viroids and an isolated hammerhead ribozyme (54), in response to high temperature and high pressure effects.

Raman scattering effect occurs when light encounters a non-homogeneity scattering material and interacts with the electron cloud and the bonds of that molecule. The inelastic scattering of the incident light resulting in a change in frequency of the incident photons is known as Raman scattering. Raman spectroscopy measures the intensity of the scattered light. If the frequencies of the scattered photons have lower frequencies than the initial radiation, then the Raman lines are referred to as Stokes bands and those that have higher frequencies are known as anti-Stokes bands [10]. Stockes Raman scattering is widely used as the intensities of the Raman bands are higher than anti-Stokes Raman scattering bands. The frequency of each Raman band in the Raman spectrum is characteristic of a particular vibration mode on the molecule. The vibrational modes of a molecule are then sensitive to the atomic and functional group composition, as well as the environments and the interactions of these groups. Vibrational spectra contain a great deal of information about the molecular structure and dynamics of RNA [11,12]. Raman spectroscopy has a great potential to probe molecular structures, not only of highly concentrated fibrous forms but also of diluted nucleic acid solutions under near-physiological conditions [13]. The common goal in such investigations is to establish a reliable correlation between vibrational spectra and specific structural features of RNAs and their biologically important complexes. In particular Raman vibrational modes of the RNA phosphodiester group and base rings are sensitive to the conformation of the RNA backbone [13,14] Libraries of empirically established correlations between Raman spectra and biologically important active nucleotide structures in the A, B and Z forms have been compiled [15], although some correlations involving Raman conformation markers of RNA structures are as yet not fully interpretable and are being intensively investigated. Nevertheless, correlation between Raman vibrational spectra and specific structural features of RNA from *Avocado Sunblotch* viroids (ASBVd) have been clearly established in this manuscript.

High Pressure is an interesting tool to shift equilibrium of multi component systems towards more compact states and to perturb their associated kinetic properties. Variations in «reaction volume» as well as «activation volume» associated with all these « conformers » can be deduced from the « Le Chatelier » principle [16,17]. High pressure physico-chemistry studies are used as a tool to probe the stability and dynamics of macromolecules to understand structural transformations in these macromolecules and their biologically relevant properties [18-20]. Detection of reaction equilibrium and kinetic changes are obtained usually by observation of some spectroscopic variables (absorption or fluorescence) under pressure. Such technique requires demonstration that the observed changes do not arise as a result of direct effect of pressure on the chromophore or fluorophore. In addition, an optical method for the measurement of enzyme kinetics is not always available. We have previously developed a reactor permitting to directly sampling-out products at any pressure for steady state studies of enzyme kinetics [21]. Initially, the pressure is maintained constant manually through a high pressure generator. In the present study, during the sampling-out of products, the pressure of the reactor can be kept constant by a programmable remote-controlled motor of the generator. Because aqueous solution is non compressible, during sampling-out a drop of the pressure will occur which perturbs the accuracy of the measurements. Gel electrophoresis analysis is then used to measure the fraction of the cleaved products as a function of time at any pressure and temperature under study.

The RNA from *Avocado Sunblotch* viroids (ASBVd) is an excellent model for such study. They are the smallest pathogens of plants characterized by a compact rod-like circular RNA 246-475 nucleotides long [22]. They have no envelope, no capsid, so that the Raman signals are not contaminated by the capsid proteins. *Avocado sunblotch* viroids (ASBVd) belongs to the Avsunviroidae familie, that does not code for any protein and possesses a catalytic RNA with a hammerhead ribozyme (HHR) motif responsible for a crucial cleavage step during viroid replication. Metal ions are involved in HHR activity within the cleavage sites (C-U and C-G) [23,24]. Cleavage is a transesterification reaction that converts a 5', 3' diester to a 2', 3' cyclic phosphate diester via an SN2 mechanism [25]. During replication, (+) and (-) complementary strand sequences are generated from ASBVd through the symmetric rolling circle mechanism [26]. The analysis of the ASBVd contents in avocado extracts [27] revealed the presence of RNA of both polarities in multimeric forms, from monomers to octamers for ASBVd(+) and monomers to dimers for ASBVd(-). It has been shown that complexes between viroids and specific tRNAs exist under physiological conditions. The fact that the concentrations of tRNAs and viroids may be sufficiently high in the cell, suggests that these complexes may also be formed *in vivo* with functional relevance [28]. Because of the diversity of structures and dynamics that participate in viroid trafficking within the cell and between cells, as well as during infectivity, it is of crucial interest to characterize the structural elements involved in viroid processing. These viroid structural components might represent the driving force necessary to penetrate the cell as well as to interact with cell components. Furthermore, structural elements possibly correspond to functional changes during the life cycle of the viroid [29,30]. Despite the large amount of information

regarding the molecular biology of Avsunviroidae, to date little is known regarding the structure and conformational aspects of the cleavage of (-) and (+) ASBVd strands and the catalytic role of Mg^{2+} for efficient self-cleavage of such viroids [12].

Materials and Methods

Plasmid construct and viroid preparation

Plasmid pBmASBVd was constructed by cloning the monomer ASBVd sequence into the PKS plasmid, restricted by the EcoR1 and BamH1 enzymes, and the monomer sequence was extracted from the plasmid pBdASBVd containing a dimeric viroid cDNA [46]. Viroids were prepared by *in vitro* transcription. DNA templates used for transcription to synthesize the (-) and (+) ASBVd viroids, were PCR amplification products using respectively the oligonucleotides sense 5'-TAATACGACTCACTATAGGAAGAGATTGAAGACGAGTG-3' containing the T7 promoter (underlined) and antisense 5'-GATCACTTCGTCTCT TCAGG-3' or the oligonucleotides sense 5'-AAGAGATTGAAGACGAGTG-3' and antisense 5'-TAATACGACTCACTATAGGGATCACTTCGTCTCTTCAGG-3' containing the T7 promoter (underlined) as primers in the presence of the pBmASBVd plasmid. The cDNAs recovered were precipitated with ethanol, and the resulting pellets were dissolved in water. The transcription reactions performed by the T7 RNA polymerase were carried out overnight at 37°C in a final volume of 5 ml containing transcription buffer, each rNTP, and RNase inhibitor (Fermentas). The transcriptions were stopped by treatment with RNase-free DNase I (Fermentas) for 30 min at 37°C, to degrade the DNA template. RNAs were precipitated with ethanol and resuspended in water containing 0.05% xylene cyanol and 50% deionized formamide. The resulting mixture was denatured for 2 min at 65°C prior to fractionation by denaturing (7 M urea) 10% polyacrylamide gel electrophoresis (PAGE, 19:1 ratio of acrylamide/bisacrylamide) using TBE buffer. Transcripts were detected by UV shadowing and the bands corresponding to the 247 nt full length fragments of both polarities were excised, the RNA eluted overnight in 300 mM sodium acetate, pH 5.2, filtered through 0.22 µM filters, ethanol precipitated and dried. After dissolving in ultrapure water, the RNAs concentrations were determined by UV absorbance (NanoVue GE Healthcare) and the samples were stored at -20°C.

Gel electrophoresis experiment

Kinetic of the viroids cleavages were followed at 45°C in 50 mM cacodylate buffer (or D_2O buffer), pH 7.2 in the presence of 150 mM KCl and 20 mM Mg^{2+}. For high pressure experiments at several temperatures, Tris buffer was used. 35 ml of incubated solution was sampling-out every 5 mn till 120 mn. Aliquots were removed from the incubated samples in the high pressure bio-reactor at various times and quenched in one volume of stop solution (7 M urea, 50 mM EDTA, pH 7.5 and 0.01% xylene cyanol) to determine the fraction of the cleaved products at 25°C. The total experiment lasted 2-3 hours. Aliquots were then loaded onto a denaturing gel (6% SDS-PAGE) for analysis.

Raman instrumentation and experiment

Because Raman scattering is typically very weak and the difficulty is to separate the weak inelastic scattering light from the intense Rayleigh scattering laser light. A new home-built near-infrared (NIR) Raman spectroscopy is setup which is more sensitive and because the use of an near-infrared excitation at 780 nm (a double photon excitation) permits to avoid excitation of fluorescence emissions. Briefly, the excitation light at 780 nm was provided by continuous wave Ti:Sapphire laser (Spectra Physics, model 3900S) pumped by an argon-ion laser (Spectra Physics Stabilite 2017). The configuration of the excitation optics is shown in **Figure 1**.

Figure 1 : Configuration of the laser excitation optics in the NIR raman spectroscopy setup. Laser 1 is an argon-ion laser (Spectra Physics Stabilite 2017) used to pump a continuous wave Ti:Sapphire laser 2 (Spectra Physics, model 3900S). The output Laser at 780 nm (in red) is used to excite the viroid solution in a sample cell. The spectrograph (Acton SpectraPro 2500i) is coupled with deep-depletion back-illuminated NIR CCD (Princeton Instruments SPEC-10 400BR/LN).

The details of the NIR-Raman spectroscopy detection system is shown in **Figure 2**.

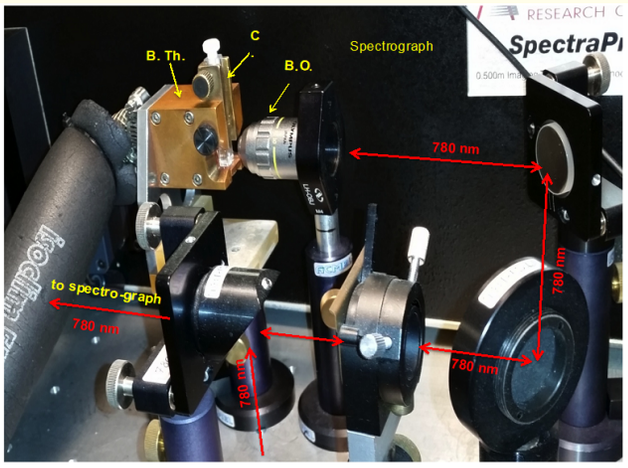

Figure 2 : Light paths of the sample's optical excitation system (in red) and Raman light scattering detection system in the NIR Raman spectroscopy setup. (B.O.) is an infinity-corrected long working distance objective (Olympus MA10, M= 10X, NA = 0.25). (C.) is a quartz sample cell (external dimensions 10x10x40 mm, internal dimensions 2x2x35 mm). (B.Th.) is a block in brass, surrounding the cuvette to thermostate the sample cell from +5 to 95°C + /- 0,5°C. Near infrared (780nm) excitation power was directed into the sample cell (C.) through an objective (B.O.) used to collect the Raman signal in a backscattering geometry and to deliver it onto the spectrograph (Acton SpectraPro 2500i) coupled with deep depletion back-illuminated NIR CCD (Princeton Instruments SPEC-10 400BR/LN). The Raman light was focused on the spectrograph entrance by an achromatic lens with f = 75 mm.

Laser light was focused into the specifically designed quartz sample cell (external dimensions 10x10x40 mm, internal dimensions 2x2x35 mm) filled with viroid solution (10-20 µ l) by an infinity-corrected long working distance objective (Olympus MA10, M= 10X, NA = 0.25). Excitation power was attenuated to ~300 mW in the sample cell. The same objective was used to collect the Raman signal in a backscattering geometry and to deliver it onto the spectrograph (Acton SpectraPro 2500i) coupled with deep depletion back-illuminated NIR CCD (Princeton Instruments SPEC-10 400BR/LN). The Raman light was focused on the spectrograph entrance (slit width 30 µ m) by an achromatic lens with f = 75 mm. The Raman signal was separated from the laser light by two Semrock RazorEdge long pass filters (grade U). One filter, with λ_{laser} = 780 nm, was placed perpendicularly to the optical beam just before the focusing lens, another one with λ_{laser} = 830 nm was used as a dichroic beamsplitter at an angle of incidence of 45°, it reflects laser light at 780 nm and transmits all the wavelengths longer than 785 nm.

Raman spectra were acquired with the WinSpec software, further data treatment was performed using Igor Pro for Windows software. To obtain the viroid Raman spectrum, the contributions from the PBS and quartz cell were subtracted from the recorded spectrum, normalized on the water bending band around 1640 cm^{-1}. Spectral resolution of Raman experiments was ~5 cm^{-1}. Frequency calibration was performed using Raman lines of toluene with absolute accuracy ±2 cm^{-1} and relative frequency position accuracy better than ±1 cm^{-1}. The total accumulation time for one Raman spectrum was 10 to 30 min depending on the sample studied.

For Raman experiments, 800 µg of dry RNA were suspended in 10 µl of water and denatured at 95°C for 45 s and then slowly (3°C/min) renatured by cooling to 20°C. Salts and buffers were adjusted to the experimental conditions in a total volume of 10-20 µL. The final viroid concentration in the sample cell varied between 0.63 and 1 mM. The standard aqueous cacodylate buffer used in Raman experiments (if not indicated otherwise) was the following: 20 mM sodium cacodylate pH 7.2, 150 mM KCl, without Mg^{2+}, at 20°C. The standard deuterated aqueous cacodylate buffer was the following: 20 mM sodium cacodylate pH 6.8, 150 mM KCl, no Mg^{2+}, at 20°C. The sample cell was thermostated within ±1°C. For measurements at elevated temperatures, a thin layer of oil was accurately poured on top of the sample solution to prevent evaporation.

High pressure bio-reactor

Theory of pressure and temperature effects

High pressure is usually chosen as a convenient tool to probe enzyme stability and activity to examine the mechanism by which enzymes catalyzed reactions. Following the Le Chapelier-Braun's principle an increase of hydrostatic pressure shifts the equilibrium of multi component systems towards more compact state and accelerates the rates of the process [31,32].

Thermodynamically, the reaction volume and activation volume are expressed as

$$(\partial \ln K/\partial P)_T = -\Delta V°/RT \quad \text{.....(1)}$$

$$(\delta \ln k/\delta P)_T = -\Delta V^{\ddagger}/RT \quad \text{.....(2)}$$

Where K is the equilibrium constant, P the pressure in MPa, R the universal gas constant (8.314 J mol^{-1} K^{-1}), T the absolute temperature in °K and ΔV° the reaction volume change (ml/mol) which is equal to the difference between the partial molar volumes of the products and the reactants, at constant temperature. k is the rate coefficient and $\Delta V^{\ddagger}$ the activation volume (ml/mol) at constant temperature which is the pressure derivative of the change in activation free energy ($\Delta G^{\ddagger}$) at constant temperature.

The origin of the reaction volume change is a complex contribution of several volumes

$$\Delta V°_{app.} = V°_{intr.} + V°_{cav.} + V°_{solv.} \quad \text{.....(3)}$$

Where $V°_{intr.}$ is the constitutive atomic volume. The presence of void volume ($V°_{cav.}$) and differential hydration volume ($V°_{solv.}$) are responsible for negative volume changes in the reaction [33]. Regarding the reaction rate constants, positive activation volume indicates a decrease of the observed rate (k_{obs}), while a negative activation volume indicates an acceleration of the observed rate (k_{obs}).

In the case of a non-linear behavior of $\ln k_{obs}$ versus pressure, the observed rate (k_{obs}) is expressed by a quadratic equation [34]

$$\ln k_{obs.} = \ln k_0 - (\Delta V^{\ddagger}/RT)\, P + (\Delta \beta^{\ddagger}/2RT)\, P^2 \quad \text{.....(4)}$$

Where $\Delta\beta^{\ddagger}$ is the activation isothermal compressibility (MPa^{-1}), k_{obs} and k_0 are the rate constants respectively at high hydrostatic pressure and normal pressure, P the pressure in MPa, R the universal gas constant (8.314 J mol^{-1} K^{-1}), T the absolute temperature in °K.

Temperature is also an interesting parameter to probe the structure and function of enzymes .The behaviour of reaction rate constants is governed by the Eyring-Polanyi equation [35,36]. Energy barriers for conformational dynamics and enzyme catalytic turnover is expressed as

$$\ln (k/T) = - (\Delta H^{\ddagger}/R) \,.\, I/T + \ln(k_B/h) + \Delta S^{\ddagger}/R \quad \text{.....(5)}$$

where k is the rate coefficient, T the absolute temperature, $\Delta H^{\ddagger}$ the activation enthalpy, R the universal gas constant, k_B the Stefan-Boltzman constant (1.381 10^{-23} J K^{-1}), h the Planck's constant (6.626 10^{-34} J s) and $\Delta S^{\ddagger}$ the activation entropy.

The comparision between Arrhenius equation and Eyring equation gives the following relation

$$E_a = \Delta H^{\ddagger} + RT \quad \text{.....(6)}$$

where E_a is the activation energy barrier of reaction. Low value of E_a and $\Delta H^{\ddagger}$ leads to fast rates, high value of E_a and $\Delta H^{\ddagger}$ leads to slow rates. Typical values of E_a and $\Delta H^{\ddagger}$ lie between 20 and 150 kJ/mol.

High pressure-temperature bio-reactor instrumentation

A schematic diagram of the high pressure-temperature bio-reactor system is shown in **Figure 3**. The reactor is composed of a cylindric stainless steel block made of Iconel 718, the dimensions of which are : $Ø_{ext.}$ = 73 mm, long = 108 mm. A reaction chamber of dimensions $Ø_{ext.}$ = 97.5 mm and $Ø_{int.=}$ 10.5 mm is drilled inside the block. A high pressure piston with Bridgman's o-ring sealing is included inside the chamber allowing the increase of pressure in the chamber till a maximum of 400 MPa. The total volume of the reaction chamber is about 5.3 ml. The pressure is controlled through a programmable motor remote-controlled driver of the pump (Top Industrie). The compression chamber is surrounded by a circulating brass room for temperature control from 5 to 95°C +/- 0.5 °C. The bottom of the reactor communicates to a high pressure sasse of small and fix volume (35 µl), through a high pressure valve (reactor lock). The end of the sasse are closed by two high pressure two-way valves (Top Industrie). One valve (sasse lock 1) communicates to a pressurized nitrogen tank to purge the solution out of the sasse. The second valve (sasse lock 2) allows to collect the solution inside the sasse into a reaction stop solution. The RNA from *Avocado Sunblotch* viroid (ASBVd) solution is first incubated inside the reaction chamber at a desired temperature. Then the substrate or the activator (20 mM Mg^{2+}) is introduced quickly in the reaction chamber through a small pressure-driven pump (Top Industrie). Initially, the pump is isolated from the reaction chamber by a high pressure two-way injection's valve. The reactants are mixed with a magnetic stirrer and the pressure is increased rapidly at a desired value. 35 µl of the reactant mixture are sampling-out every 5 mn till 120 mn, into the sasse by opening the reactor lock. Then such lock is immediately closed. Lock 1 and 2 of the sasse are then opened to allow the purge of the reactant mixture into a stop solution (quenched solution) composed of 7 M urea, 50 mM EDTA, and 0.01% xylen Cyanol at 25°C. Each alicot is then loaded onto a denaturating gel (6% SDS PAGE) for the determination of the fraction of cleaved products by gel electrophoresis analysis. Because aqueous solution is not compressible, each sampling-out of the reaction mixture from the reactor chamber will drop the pressure of the experiments, leading to some errors in the experiments. The designed compression reactor described in this manuscript has the advantage as compared to the previous setup [21], to automatically correct the dropping of pressure during sampling-out to keep constant the experimental pressure.

Figure 4 shows the details of the different components of the pressure-temperature bio-reactor with sampling-in of substrates and sampling-out of products.

The reactor (A) was coupled with a 400 MPa high pressure pump. Both reactor and pump were driven by an electric motor (C) related to a programmable remoted-controlled driver (D) from Top Industrie. The temperature of the reactor was controlled through

a circulating fluid (K) from the thermostat with an accuracy of +/- 0.5 °C. (E) is the high pressure transducer while (F) is a normal or high pressure syringe used to inject the activator. The bottom of the reactor was communicated to a sasse (H) of fixed volume (35 µl) which was isolated from the reactor through a lock (SL) and the two extremities of the sasse were closed by high pressure two-way valves (S1 and S2). The solution of the sampling-out reactants were purged by a pressurized nitrogen tank through a system of manometer and valves (I). A detailed view of the reactor-high pressure pump is shown in the right side of **Figure 4**, where (L) is gear

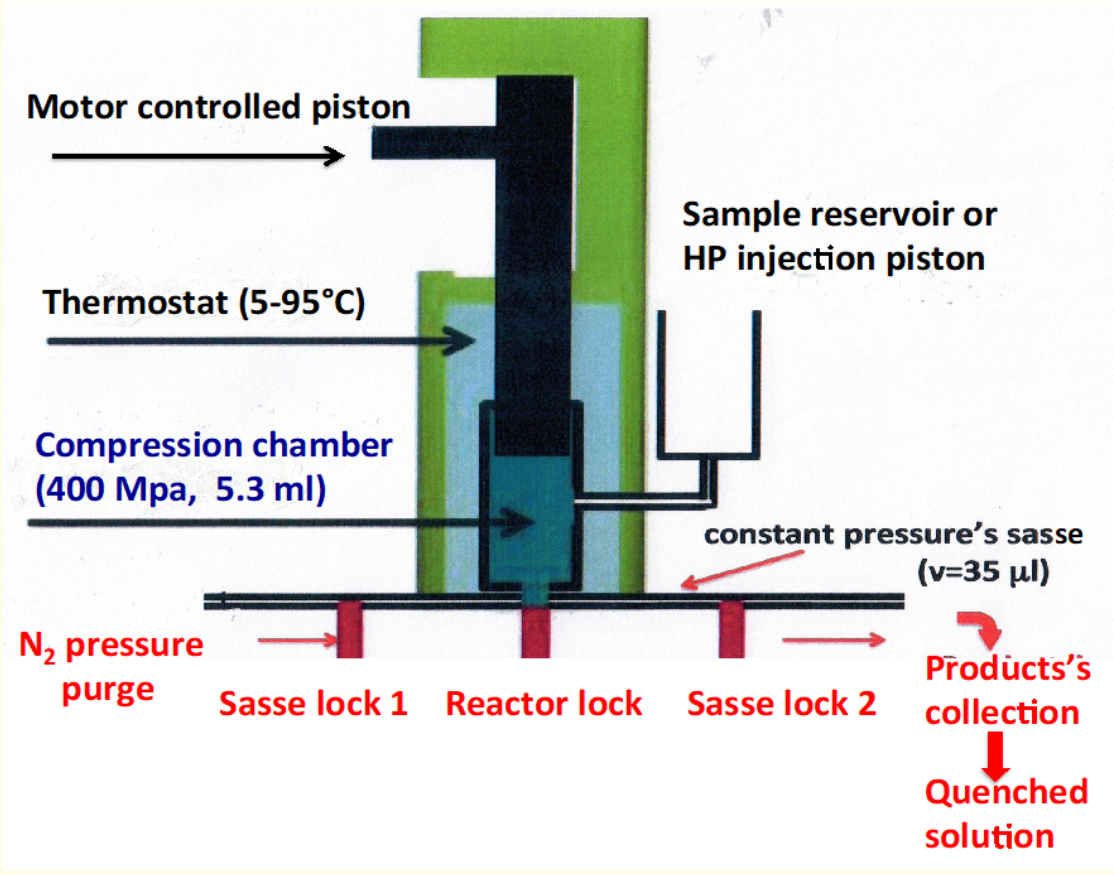

Figure 3: Principle of direct sampling-in and - out bio-reactor at constant pressure and controlled temperature.

The compression chamber is drilled inside is a cylindrical stainless steel block (made of Iconel 718, $Ø_{ext.}$ = 73 mm, long = 108 mm). The dimensions of the compression chamber has a $Ø_{ext.}$ = 97.5 mm and $Ø_{int.=}$ 10.5 mm, the volume of which is about 3.5 ml. A high pressure piston with Bridgman's o-ring sealing is included inside the chamber allowing to increase the pressure of the chamber till a maximum of 400 MPa. The piston is electrically driven by a programmable remote–controlled motor (Top Industrie). The temperature of the compression chamber can be regulated from 5 to 95 °C +/- 0.1 °C through a circulating fluid of the thermostat. The injection of the reactants can be operated through a normal syringe or through a home made high pressure piston (HP injector from Top Industrie) when the injection is required at high pressure. The originality of such a design is the existence at the end of the chamber of a sasse of small and fixed volume (35 µl) to receive the sampling-out reactant's volume at any pressure. Several high pressure valves (sasse lock 1 and sasse lock 2 and reactor lock) control the sampling-out operation. The products of the reaction in the sasse was purged out through a pressurized nitrogen tank and then the solution was stopped by a quenched solution (see materials and methods) for electrophoresis analysis of the products. To avoid the drop of pressure at each sampling-out operation, a programmable remote-controlled driver (Top Industrie) was used to keep automatically constant the pressure.

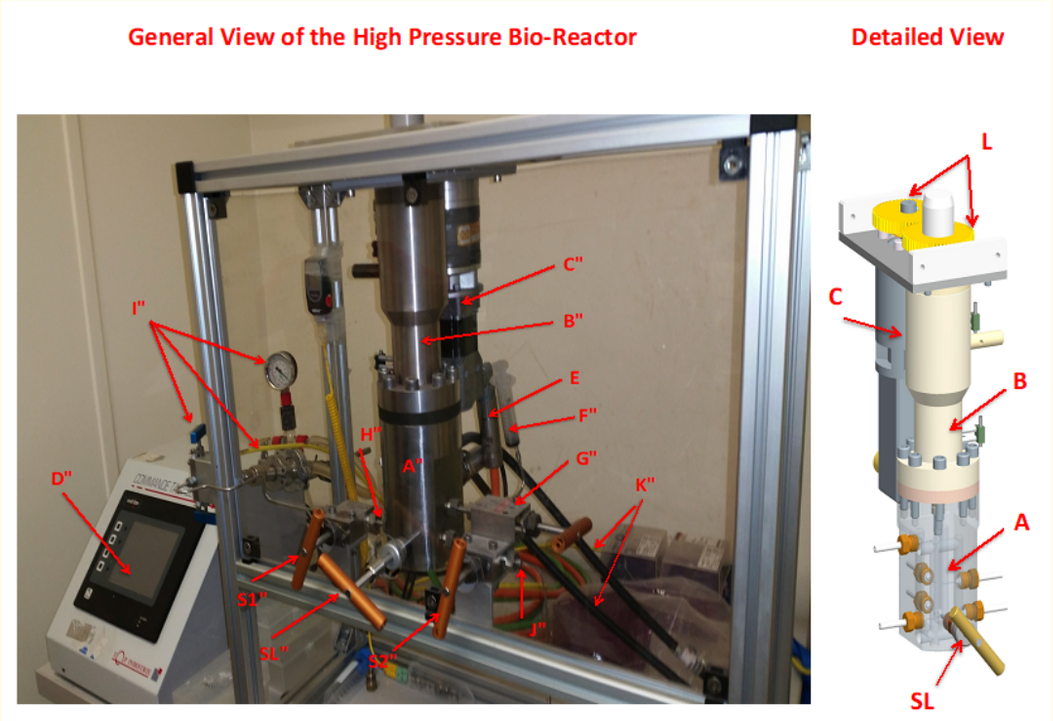

Figure 4 : The home made high pressure-temperature bio-reactor allowing sampling-in of substrates and sampling-out of products. All the different components are realized by Top Industrie. (A) is the cylindrical reactor chamber (volume of 5.3 ml) made of stainless steel (Iconel 718) allowing the chamber to resist till 400 MPa. (B) is a 400 MPa high pressure pump equipped with a Bridgman o-ring system for sealing. Such pump is connected to a special electric motor (C) (Top Industrie) to control automatically the pressure of the chamber. (D) is the programmable remoted-controlled driver (Top Indiustrie). The pressure is measured throuh a pressure transducer (E). (F) is a syringe used for normal pressure operation. For high pressure injection operation a small home made high pressure pump (Top Industrie) replaces the normal syringe. The injection volume (< 0.8 ml) is controlled by a 2-ways high pressure valve (G). (H) is the high pressure sasse isolated from the high pressure chamber by a 3-ways high pressure valve (SL). Opening of this valve (SL) allows the sampling-out of reactants at constant pressure and temperature, into the sasse. The two ends of the sasse is closed by two valves (S1: sasse lock 1 and S2: sasse lock 2). (I) is the exit of the valve (S2) for collection of the reactant's solution into a quenched solution to stop the reaction. (J) is a system of valve and manometer of the nitrogen tank used to purge the sasse. (K) is the tubing of the thermostated fluid-in and fluid-out. On the right side of **Figure 4**, is a detailed view of the high pressure reactor. L is the coupling gear wheel.

wheels to couple the motor and the pump.

Results and Discussion

Impacts of the extreme physico-chemical parameters on the structure of RNA from *Avocado Sunblotch* viroids (ASBVd)

Raman spectra and assignments of the Raman markers

Raman spectra of ASBVd polarity (-) and (+) in a standard aqueous cacodylate buffer and in the absence of magnesium (20 mM Mg^{2+}), at 20°C are shown in **Figure 5**. The Raman spectra exhibit about 30 well-resolved lines that arise from the vibration of sugar-phosphate backbone of the RNA and nucleotide bases [37]. Different types of RNA possess rather similar lines except that their intensities and frequency's positions are different, depending on each cooperative docked structure [38-40].

Several well resolved Raman lines can be assigned as RNA's structural markers.

Raman markers of the nucleotide heterocyclic rings and phosphodiester backbone linkage

Stretching vibrational frequency of purine (G) base is located at 669 cm^{-1} the intensity of which is weaker than that of base (A) located at 727 cm^{-1}. The characteristic of these Raman lines are dependent on the local conformation of the nucleotides [41]. Because the glycosidic bond (N-C1') is close to the base moiety, there

is appreciable vibrational coupling between the weak stretching vibration of the guanine and the stronger one of the ribose. Thus the intensities of Raman lines may vary depending on the geometry of the nucleotide bases ("syn" or "anti" overall rotation geometry with respect to the sugar) [42]. These lines can provide information about the torsional rotations of the glycosyl bonds and their flexibility. The stretching vibration mode at 727 cm^{-1} for purine bases in ASBVd(+), exhibits a moderate decrease in intensity (about 15%) as compared to that in ASBVd(-), **Figure 5(a)**. This can be interpreted as a ring vibrational coupling difference between purine bases and ribose in ASBVd(+), leading to a small local difference in the sugar puckering conformations, and suggesting the existence of a more compact and rigid geometry in the backbone of ASBVd(+). In addition guanine nucleotide stretching vibration around 669 cm^{-1} is assignable to C3'-endo/anti conformation ("N-type"), while the C3'- endo/syn orientation of any G base with respect to its adjacent sugar is characterized by Raman marker located at 1320 cm^{-1} [42]. Raman spectrum of free ASBVd(-) in **Figure 5(a)** shows the presence of a strong Raman line at 1252 cm^{-1} (I^{-}_{1252} = 0.84) and a weaker Raman line at 669 cm^{-1} (I^{-}_{669} = 0.3).

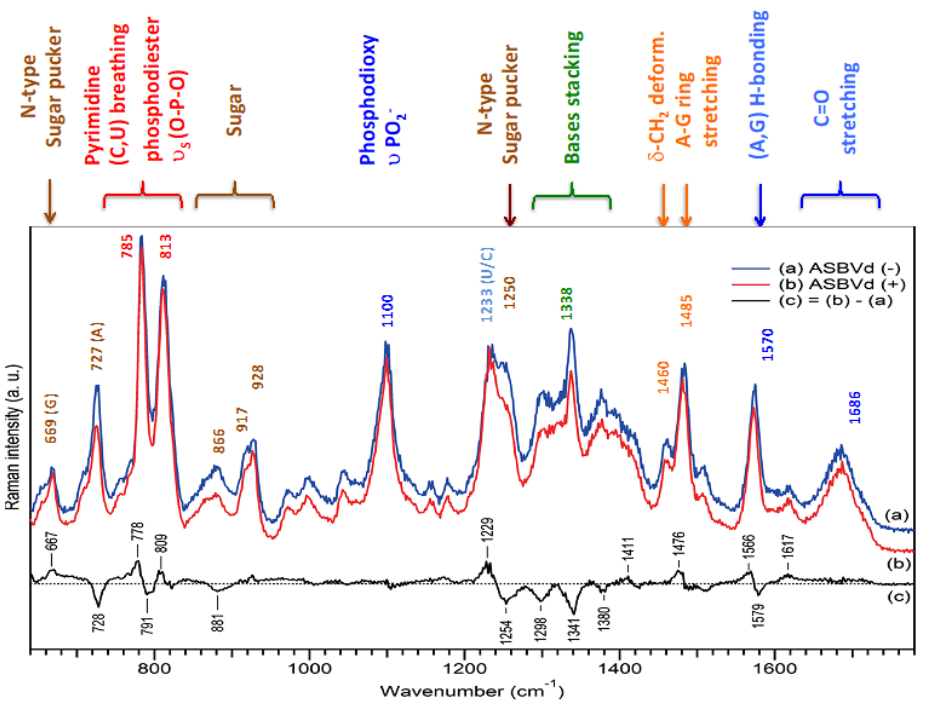

Figure 5: Assignment of major Raman lines of ASBVds. Raman spectra of ASBVd(-) ((a), blue curve) and ASBVd(+) ((b), red curve) are obtained in aqueous cacodylate buffer, in the absence of Mg^{2+}. Both spectra were normalized using the Raman line at 1100 cm^{-1} taken as an internal intensity standard, and the contributions from the cacodylate buffer and quartz cell were subtracted. The black curve (c) is the difference Raman spectrum obtained by (1:1) subtraction of the spectrum (a) from spectrum (b). The difference spectrum (c) was multiplied by a factor of 3 to visually enhance the resulting spectral changes. (with the permission of BMC Biophysics (BioMed Center) (37).

Both lines being assignable to nucleotides in C3'-endo/anti conformations. The same vibrational stretching lines are also observed in ASBVd(+) **Figure 5(b)**, with only slightly difference in intensities (I^{+}_{1252} = 0.79 and I^{+}_{669} = 0.39).

One characteristic feature in this region is the existence of two strong and sharp Raman lines, respectively at 785 cm^{-1} and 813 cm^{-1}. The Raman line at 785 cm^{-1} is assigned to ring breathing of pyrimidine (C, U) bases [43,44], and the Raman line at 813 cm^{-1} is attributed to a symmetric stretching vibration ν_s (C–O-P-O-C) of the phosphodiester linkage of the RNA. Both the intensities and frequencies of the Raman lines are sensitive to bond angle deformations of the RNA backbone [44-46]. They are being independent on base composition [45]. Normalization of the intensities of these

lines to the intensity of the phosphodioxy line ν(PO^{2-}) at 1100 cm^{-1} allows to estimate the double helical content (amount of secondary structure)

$$r_2 = I_{813}/I_{1100} \quad \text{.....(7)}$$

It was shown that for completely ordered polyribonucleotides, the value of r_2 = 1.64 [47], while for completely disordered structures, the r_2 value approaches zero [51,52]. Thus the ratio r_2 can be converted into % of ordered polyribonucleotides by using the factor 1.64 as a coefficient of division, leading to respectively 76% and 78% helical content for ASBVd(-) and ASBVd(+).

Our results are to be compared to those of Thomas., *et al.* [47] that give respectively the values of 95%, 85%, 87% helical content for 16S rRNA, 23S rRNA and R17 RNA. The secondary structures of these RNAs are more ordered and structured than in the case of ASBVd viroids.

As the intensities of the Raman lines at 785 cm^{-1} and 813 cm^{-1} vary relatively to each other at different RNA configurations, we can define a conformational parameter (degree of « A-type » phosphodiester conformation) as

$$r_{conf.} = I_{785}/I_{813} \quad \text{.....(8)}$$

Where I_{785} is the intensity of the ring breathing vibration of pyrimidine (C, U) bases, while I_{813} is the intensity of the symmetric stretching vibration of the phosphodiester linkage ν_s (C–O-P-O-C). In order to overcome the spectral overlap problem between these lines, we have adopted the method based on peak heights for the estimation of $r_{conf.}$ The conformation of the sugar-phosphodiester group of ASBVd(-) is characterized by a value of $r_{conf.}$ = 1.14. Interestingly, for a canonical « A-form » RNA, the Raman doublet 785/813 cm^{-1} exhibits typically higher Raman intensity for 811–813 cm^{-1} line as compared to that at 785 cm^{-1} line leading to $r_{conf.}$ < 1. For soluble DNA in a "canonical" B conformation, the Raman line at 813 cm^{-1} is converted into the broad shoulder at 835 cm^{-1} leading to $r_{conf.} \rightarrow \infty$. However, in the presence of low salt and 75% humidity, the symmetric phosphodiester line at 813 cm^{-1} appears in DNA fiber, yielding a $r_{conf.}$ = 1 [14]. The same conformation was found for ribozyme D5-PL-RNA where $r_{conf.}$ = 1.01 [39]. The difference in the $r_{conf.}$ parameter between ASBVd(-) and fiber DNA indicates that although both nucleic acids are in the « A-type » conformation, they differ in subtle bond-stretching vibrations located in the -C-O-P-O-C- networks and possibly also in the ribose ring [39,45]. Higher value of $r_{conf.}$ = 1.6 was found in the structure of formylmethionyl-tRNA [38], although it exhibits similar ordered secondary structure (r_2) as compared to ASBVd. This result can be interpreted by a difference in the local phosphodiester conformation of the « A-type » structure. It is to note that $r_{conf.}$ for ASBVd(+) in **Figure 5(b)** is the same as for ASBVd(-), while a slight frequency downshift is observed in the -C-O-P-O-C- vibrational mode at 813 cm^{-1} **(see Figure 5(c))**, indicating a slight difference in the rigidity of the phosphodiester backbone of ASBVd(+). On the contrary, the phosphodioxy stretching mode at 1100 cm^{-1} in both minus and plus strands remains the same, both in intensity and frequency.

Sugar and phosphoionic stretch frequency markers

Several weaker lines (866, 917, 928 cm^{-1}) which are originated from sugar vibration modes and a strong prominent Raman line at 1100 cm^{-1} which is assigned to the symmetric ν (PO^{2-}) stretching vibration mode of the phosphoionic group appear (see **Figure 5**). The strong Raman phosphoionic line is sensitive to changes in the electrostatic environment of the phosphate groups [48]. At constant ionic strength, the phosphoionic stretching vibration mode is expected to have the same intensity for all the polynucleotides and RNA [49,50] because it is not sensitive to the sugar-phosphate diester conformational change but depends only on the number of anionic oxygen atoms and therefore it can serve as a useful internal Raman marker [45].

Raman markers of base-stacking, base-pairing and sugar puckering.

In the frequency region between 1150-1600 cm^{-1} (see **Figure 5**), there are several Raman lines which are characteristics of purine and pyrimidine coupled nucleotide vibrations. These lines are very sensitive to ring electronic vibrations and are used to define the degree of base-base stacking interactions such as

$$r_{stack} = (I_{1300} + I_{1378})/I_{1338} \quad \text{.....(9)}$$

Where I_{1300} and I_{1378} are the normalized intensities of composite vibrations of adenine or guanine ring systems ($\nu_{pyr.+imidazole}$) consisting of fused cycle of six-membered pyrimidine and five-membered imidazole ($I_{im.}$) rings, while I_{1338} is the normalyzed intensity of imidazole ring vibration alone (ν_{im} at 1338 cm^{-1}). It has been shown by Valdemaras R., *et al*. [52] that such composite factor (r_{stack}) is choosen to better characterize the base-base interactions rather than to use each base ring vibrational mode alone. For free ASBVd of both polarity, the factor r_{stack} is equal respectively to 1.35 and 1.42, indicating a slight decrease in base-base interactions in AS-

BVd(+) structure.

In the same frequency region, many characteristic Raman lines appear. Line around 1233 cm^{-1} is assigned to (U, C) ring stretching vibrations which is a strong marker upon thermal unfolding (hyperchomicity). Interesting, sugar pucker structures and the bases rotation geometries determine the conformation of the nucleotides involved in RNAs motifs. The "N-type" structure is characterized by Raman marker around 1252-1254 cm^{-1} which is assignable to C-3′ atom of the sugar in "endo" position and the corresponding base in "anti" rotation geometry. The "S-type" conformation exhibits Raman marker line around 1267 cm^{-1}, which is assignable to the C-2′ atom of the sugar in "endo" position and the base in "anti" rotation geometry (Raman tertiary structural marker). **Figure 5** shows that the RNA of ASBVd of both polarity exhibits a « N-type » structure. The ribose in the RNA is manifested by a Raman line at about 1460 cm^{-1} attributed to methylene twisting ($\nu_{t(\delta\text{-}CH2)}$). Raman lines at 1485 cm^{-1} and 1574 cm^{-1} are attributed to purine A-G cycle vibrations along the long/short axis and the hydrogen bonding of bases [53].

Raman markers of H-bonding and carbonyl C=O stretching modes

The strong Raman lines resulting from (A, G) bases ring stretching vibrations are located at 1485 cm^{-1} and the H-bonding stretching vibration is located at 1574 cm^{-1} while the H-bonding in carbonyl C=O stretching modes of pyrimidines manifest a broad band centered around 1640-1686 cm^{-1}. In ASBVd (+) the maximum line at 1686 cm^{-1} is not appreciably changed as compared to ASBVd (-), (**Figure 5**). However a slight frequency downshift at 1574 cm^{-1} is observed for the H-bonding marker between A and G bases.

Impacts of temperature-induced unfolding, deuterium solvent and self-cleavage activity on Raman structural markers

Effects on nucleotide heterocyclic rings, phosphodiester backbone and phosphodioxy stretch vibration modes

Figure 6 shows different perturbation effects on respectively the nucleotide heterocyclic rings and phosphodiester backbone linkages. The polarities (-) and (+) of ASBVd viroids exhibit similar secondary structure of a « A-type » RNA (helical content equal respectively to 78% and 76%) and similar phosphodiester conformations (r_{conf} = 1.14), while there is a slight frequency downshift in the 813 cm^{-1} and 785 cm^{-1} Raman lines indicating a slight difference in the rigidity of the phosphodiester bacbone of ASBVd(+), **Figure 6 (a)**. In addition, the existence of a Raman line at 669 cm^{-1} and 1250 cm^{-1} reveals a typically « N-type » sugar pucker conformation for both polarity of the ASBVd. **Figure 6 (b)** shows that an increase in temperature till 60°C, perturbs radically the Raman spectrum of the nucleotide heterocyclic rings and the phosphodiester backbone linkage, validating the use of such lines as characteristic Raman markers for temperature-induced unfolding process. The phosphodiester mode (815 cm^{-1}) decreases in intensity and downshifts by Δν of -15 cm^{-1}, concomitantly, a broad shoulder at 779 cm^{-1} appears. This result is indicative of a destabililization of the helical structure (loss of 27% ordered helical content) and a loss of a « A-type » structure of the RNA with the appearance of a new nucleotide conformation. In the contrary, the effects of deuterium solvent show huge changes in purine (A) (at 727 cm^{-1}) and (G) (at 669 cm^{-1}) Raman lines with frequency downshifts of Δν = - 11 cm^{-1}, **Figure 6 (c)**. The causes of such changes are the removal of coupling between ribose and purine bases upon deuteration. In the same time pyrimidine Raman line at 785 cm^{-1} downsifts to 717 cm^{-1} with an important intensity decrease indicating that a new « A-type » structure is appearing. The conformation ratio ($r_{conf.}$) decreases by 25% and the helical content (r_2) increases from 1.28 to 1.40. The result suggests that deuteration process induces a helical rearrangement to a new conformation and perturbs the internal loops interactions. **Figure 6 (d)**, shows the consequence of the self-cleavage of RNA from ASBVd on the Raman specific markers. After cleavage of the RNA, the obtained pyrimidine Raman line at 784 cm^{-1} and the symmetric phosphodiester Raman line at 813 cm^{-1} are found to be downshifted by Δν -10 cm^{-1} (-6%) and the intensity of the Raman line at 813 cm^{-1} of the phosphodiester linkage increases by 4%. These frequency downshifts are indicative of vibrational energy decreases, characteristic of some conformational changes which is a consequence of the self-cleavage transesterification that converts 5', 3' phosphodiester into 2', 3' cyclic phosphate diester [25]. In **Figure 6 (e)**, it is shown that both the sugar and phosphodioxy Raman markers are similar for ASBVd polarity (-) and (+). While increasing the temperature till 60°C, **Figure 6 (f)**, downshifts the phosphodioxy Raman line from 1100 cm^{-1} to 1087 cm^{-1} (Δν = -13 cm^{-1}) presumably due to temperature-induced changes in hydration of the charged phosphates. The small sugar Raman line at 840 cm^{-1} slightly increases. Deuteration of the RNA from ASBVd does not perturb the phosphodioxy Raman line at 1100 cm^{-1}, **Figure 6 (g)**, but slightly increases the sugar Raman line at 928 cm^{-1}. Raman lines from sugar stretch vibrations, at respectively 917 cm^{-1} and 866 cm^{-1} sligthly decreases in intensities. **Figure 6 (h)**

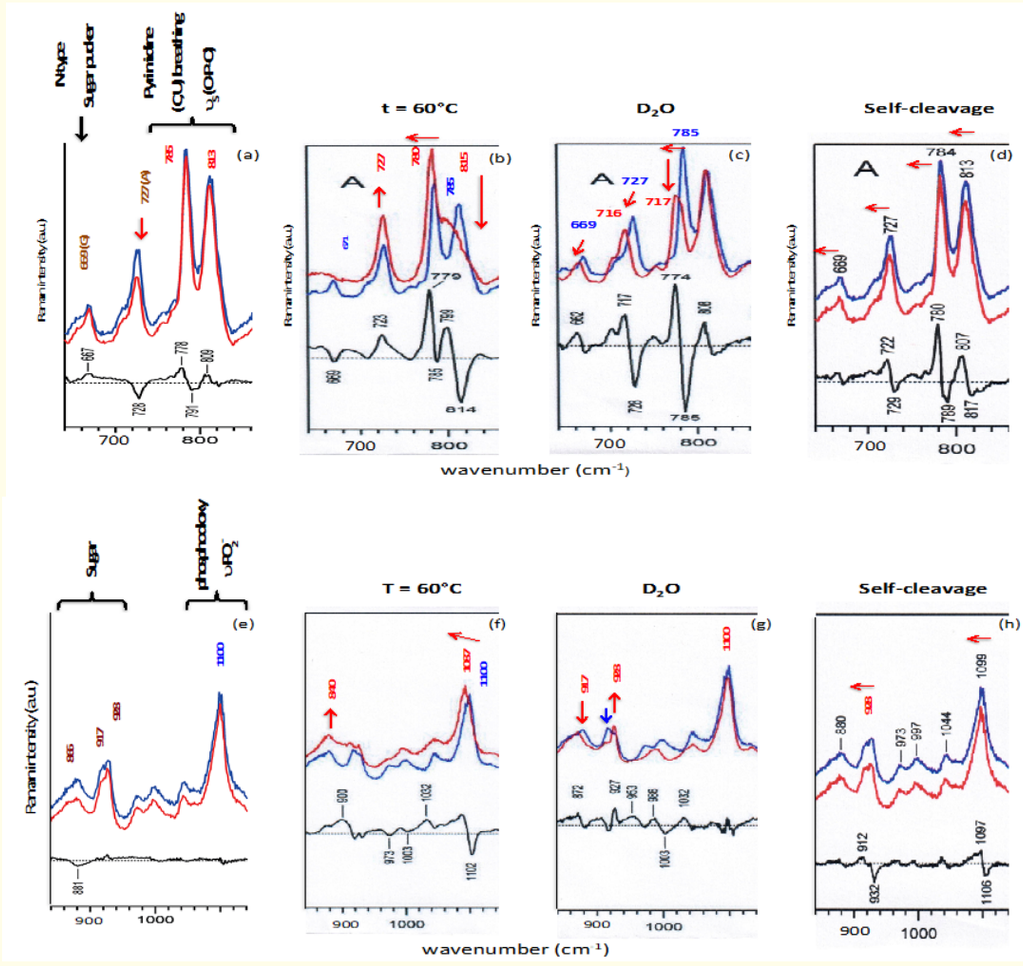

Figure 6: Effects of polarity (-) and (+) of ASBVd in panel (a). High temperature in panel (b), deuterium solvent in panel (c), and self-cleavage activity in panel (d) on Raman specific markers of RNA' nucleotide heterocyclic bases and phosphodiester backbone vibration modes of *Avocado Sunblotch* viroids. Blue curves are RNA spectra in normal conditions. Red curves are the perturbation Raman spectra. Black curves are difference spectra of red curves minus blue curves. Effects of polarity (-) and (+) of ASBV in panel **(**e). High temperature in panel (f). Deuterium solvent in panel (g) and self-cleavage activity in panel (h) on Raman specific markers of sugar and phosphodioxy stretch vibration modes of *Avocado Sunblotch* viroids. Blue curves are RNA spectra in normal conditions. Red curves are the perturbation Raman spectra. Black curves are difference spectra of red curves minus blue curves. (with the permission of BMC Biophysics (BioMed Center) (37)).

shows that self-cleavage of RNA from ASBVd induces several down-shifts of the phosphodioxy Raman line from 1100 cm^{-1} to 1099 cm^{-1} as well as the sugar Raman line at 928 cm^{-1}, presumably due to a consequence of environmental changes after the self-cleavage transesterification process.

Effects on sugar pucker, bases stacking and H-bonding stretch vibration modes

In the previous sections it is emphazised that sugar pucker is an important characteristic feature of the tertiary structure in the RNA conformation of ASBVd viroid. It defines the backbone geometry and the rotation of the bases with respect to the sugar. The so-called « N-type » sugar conformation mode is shown in **Figure 7 (a)** to exhibit a strong Raman line located at 1250 cm^{-1} in ASBVd(-) while the intensity of such Raman line decreases moderately (15%) in ASBVd(+), indicating some difference in the ring vibration coupling between purine bases and ribose. In addition, base-base stacking mode which contributes importantly to the conformation and stability of the RNA structure is characterized by a strong Raman line at (ν_{Im}) = 1338 cm^{-1} and two smaller Raman lines at 1300 cm^{-1} and 1378 cm^{-1} (composite vibrations of adenine or guanine ring systems ($\nu_{pyr.+\ imidazole}$)). The calculated base stacking ratio (r_{stack}) following equation (9), is equal to 1.35 and 1.42 respectively for ASBVd(-) and ASBVd(+). **Figure 7 (b)** shows that the « N-type » sugar pucker is strongly destabilized by increasing the temperature. At 60°C, Raman line at 1228 cm^{-1} decreases and shifts to an intense line at 1226 cm^{-1} this is interpreted as a loss of nucleotide conformation, phosphodiester backbone geometry and base-stack-

ing. **Figure 7 (c)** shows that deuteration of the mobile hydrogen of RNA does not modify the sugar pucker conformation (no changes in I_{1233}), while the intensity of Raman line of the (U, C) stretching vibration at 1233 cm^{-1} disappears upon deuteration. The intense purine (A) Raman line at 1302 cm^{-1} increases and the intensity of imidazole Raman line (ν_{Im} = 1338 cm^{-1}) decreases and shifts to 1485 cm^{-1} leading to a calculated ratio r_{stack} to increases from 1.32 to 1.66 (+34%). The imidazole ring vibration alone is slightly shifted to 1334 cm^{-1} (Δν about -7 cm^{-1}), consequence of bases stacking destabilizing. **Figure 7 (d)**, shows that sugar pucker marker, ring stretching modes of adenine or guanine and the imidazole ring vibration mode alone are very sensitive to conformational changes of RNA due to its cleavage that converts 5', 3' phosphodiester into 2', 3' cyclic phosphate diester. In **Figure 7 (e)**, It is shown that the intensities of methylene twisting stretching vibration ($\nu_{t(\delta\text{-}CH2)}$) and the (A, G) ring stretching mode (at 1460 cm^{-1} and 1485 cm^{-1}) sligthly increased in ASBVd(+) as compared to ASBVd(-), while the (A, G) H-bonding located at 1570 cm^{-1} is frequency downshifted (Δν = - 13 cm^{-1}) for ASBVd(+). The carbonyl C=O stretching line at 1686 cm^{-1} has the same intensity for both viroids. In **Figure 7 (f)**, it is shown that increasing temperature to 60°C induces several increases of Raman intensity lines, in particular a moderate intensity increase in the C=O carbonyl region is observed, reflecting a rupture of hydrogen bonds between bases. In **Figure 7 (g)**, the presence of D_2O cosolute decreases strongly the stretching vibration mode of (A, G) rings at 1485 cm^{-1} and slightly increases their H-bonding in 1570 cm^{-1}. The broad band from C=O stretching of uracil base, at 1686 cm^{-1} retreats and shows more resolved lines in 1653 cm^{-1} (unpaired uracil residues) and 1683 cm^{-1} (paired uracil residues) due to H_2O-D_2O exchanges. In **Figure 7 (h)**, several interesting frequency

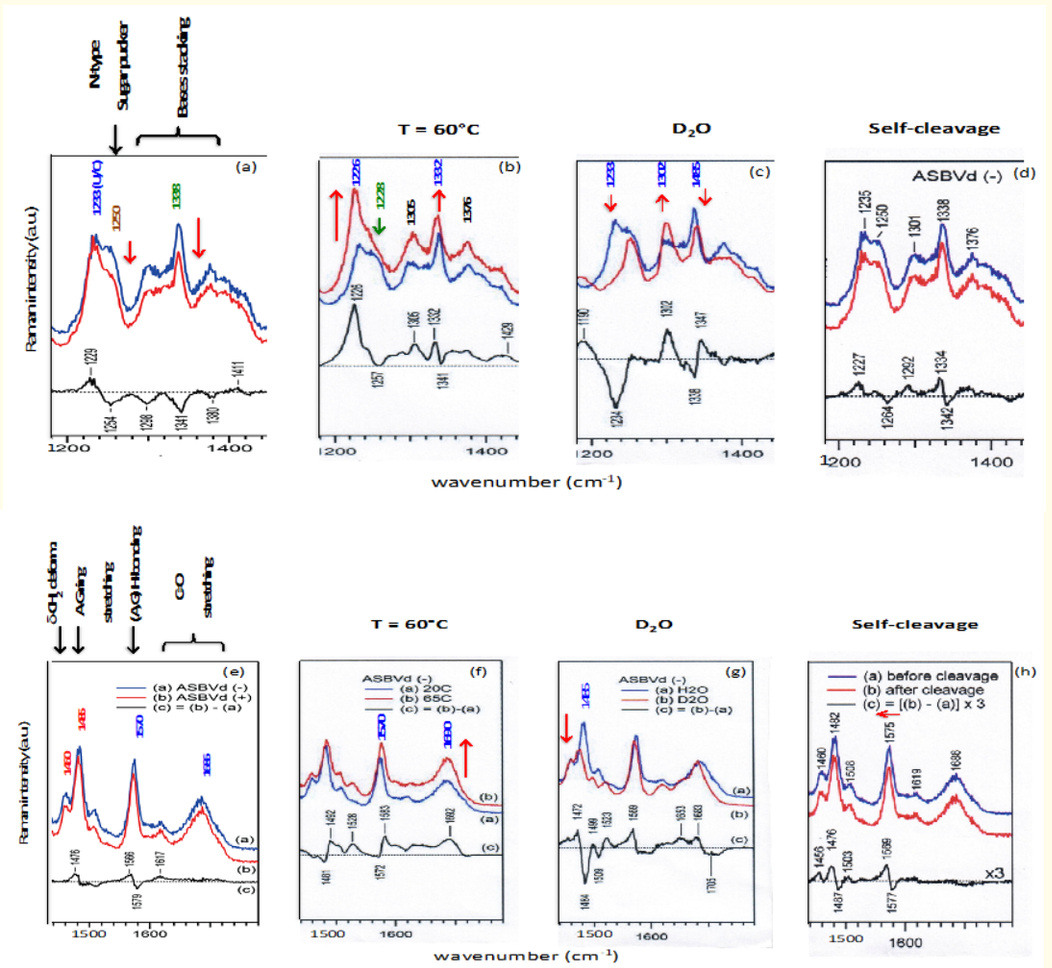

Figure 7: Panel (a) effects of polarity (-) and (+) of ASBVd on Raman specific markers of RNA's sugar pucker, bases staking stretching vibration modes of *Avocado Sunblotch* viroids. Panel (b) effects of high temperature. Panel (c) effects of deuterium solvent. Panel (d) effects of self-cleavage activity. Blue curves are RNA spectra in normal conditions. Red curves are the perturbation Raman spectra. Black curves are difference spectra of red curves minus blue curves. Panel (e) effects of polarity (-) and (+) of ASBVd on Raman specific markers of RNA's H-bonding and carbonyl stretching vibration modes of *Avocado Sunblotch* viroids. Panel (f) effects of high temperature. Panel (g) effects of deuterium solvent. Panel (h) effects of self-cleavage activity. Blue curves are RNA spectra in normal conditions. Red curves are the perturbation Raman spectra. Black curves are difference spectra red curves minus blue curves. (with the permission of BMC Biophysics (BioMed Center) (37)).

downshifts (around $\Delta\nu$ = - 8 cm^{-1}) from the rings stretching (1485 cm^{-1}) and the hydrogen bonding (1570 cm^{-1}) of (A, G) bases are observed. In addition the methylene ($\nu_{t(\delta\text{-}CH2)}$) deformation Raman line at 1460 cm^{-1} also downshifts in frequency, a consequence of RNA self-cleavage leading to some local structural conformational changes.

Impacts of cosolute, high temperature and high pressure on self-cleavage activity of the RNA from ASBVd viroids

Effects of aqueous e and deuterium cosolute on ASBVd(-) and ASBVd(+) self-cleavage activity at 45°C.

Magnesium (Mg^{2+}) plays a role of activator in the self-cleavage kinetics of RNA from ASBVd viroids. In aqueous solution at room temperature, there is no (or very slow) activity of the viroids. In the contrary at 45°C, the rates of self-cleavage kinetics are high enough to allow the study of the activity of ASBVd(-) as compared to that of ASBVd(+). Both studies are performed by gel electrophoresis at 45°C in aqueous buffer and in D_2O buffer as described in Materials and Methods. The cleaved fractions versus time at 45°C are shown in **Figure 8**. in which the kinetic curves are analysed using single exponential kinetic equation. **Figure 8 (A)** shows that the cleaved rates for ASBVd(-) is faster in H_2O buffer (k_{H2O} = 0.032 min^{-1}) than in the presence of D_2O buffer (k_{D2O} = 0.009 min^{-1}). The observed rate reduction is around a factor of 3.5. After 200 minute of reaction, the cleaved fraction equal 65% in H_2O and 32% in D_2O buffer. It is shown that deuteration perturbation is a useful tool to study the accessibility of mobile hydrogens and the implication of some of them in the acid/base catalysis process involving proton transfer. The replacement of hydrogen by deuterium atom should decrease the rate of catalysis. However, many of the mobile hydrogen are implicated in the conformation and the stability of RNA's structure through base-base H-bonding as revealed in the Raman spectroscopy study. Conformational changes near the actif site as well as the difference in structural dynamics of ASBVd(-) in different solvent environments are another factors that corroborate well with the observed difference in the self-cleavage kinetic reduction. **Figure 8 (B)** gives the self-cleavage rate profiles for ASBVd(+) viroids in H_2O and D_2O environments. It is found that in aqueous buffer, the rate of self-cleavage for ASBVd(+) is 3.2 time less rapid than for ASBVd(-). Raman spectrocopy study demonstrates that both polarity of viroids exhibit around the same secondary structure, while they differ on the self-cleavage activity. It is demonstrated that in some solvent conditions, secondary and tertiary structures can fold in a cooperative or noncooperative multistate fashion leading to an active dock structure or an heterogeneity folding structure. The two

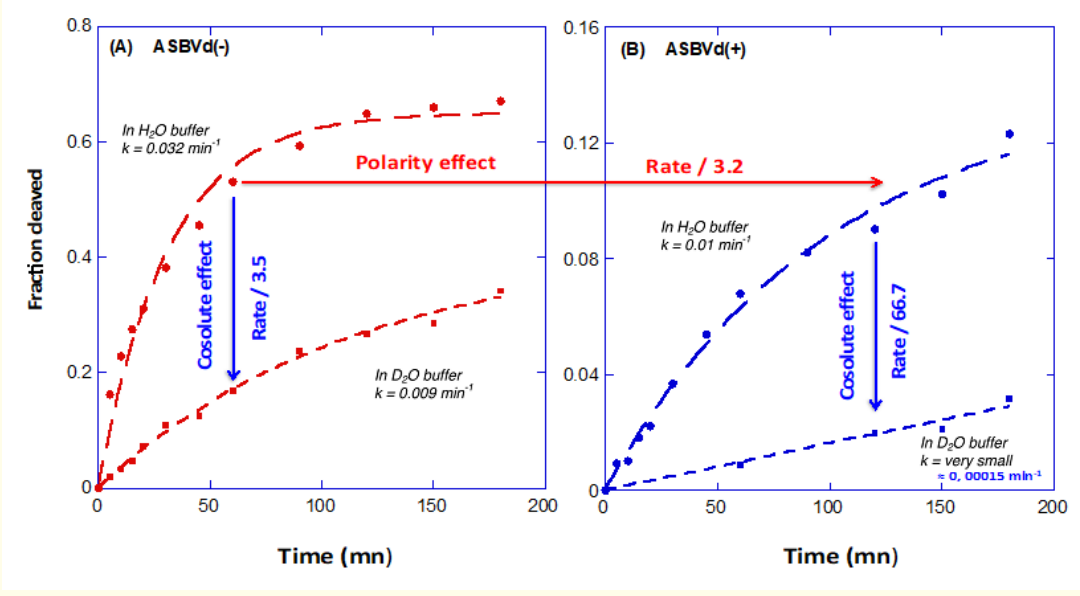

Figure 8: Effects of solvent environments on self-cleavage activities of ASBVds. The kinetic curves of fraction cleaved RNA as detected by gel electrophoresis at 45°C (see Materials and Methods), are shown in panel (A) for ASBVd(-) viroids in aqueous and D_2O buffers and in panel (B) for ASBVd(+) viroids in the same conditions of solvants. (with the permission of BMC Biophysics (BioMed Center) (37)).

overlapping mechanisms of folding can be shifted to a decrease stability of the tertiary structure and an enhancement of certain secondary structure leading to a less active RNA. Molecular crowder effects could be used to probe such hypothesis. In D_2O solvant, the activity of ASBVd(+) exhibits a huge decrease of its rate constants by shifting the rate from 0.01 mn^{-1} to 0.0015 min^{-1}, a reduction factor of 66.7 emphasizing the unstability of ASBVd structure.

Effects of high temperature and high pressure on ASBVd(-) self-cleavage activity

Figure 9 presents the effects of high temprature and high pressure on the self -cleavage activity profile of ASBVd(-). A bell-shape temperature dependence of the activity is found in **Figure 9 (a)**. An increase of the temperature at room pressure, (blue curve) accelerates the self-cleavage steady-state rates ($V_{(i)}$) of ASBVd (-) viroid untill a $T_{inact.\,(1\,bar)}$ = 55°C where the rates decreases, presumably due to temperature-induced unfolding of the RNA's structure. Analysis of the self-cleavage rates in the linear portion of the bell-shape profile, permits to obtain an energy barrier of the reaction following equations (5) and (6), to be

$E_{a\,(1bar)}$ = 9.6 kcal.mol^{-1} (40 kJ.mol^{-1}) .....(9)

Increasing pressure affects the rates of the reaction which considerably decrease but the bell-shape of the temperature profile is conserved without perturbing the inactivation temperatures ($T_{inact.\,(pressure)}$ = 55 °C). However a new activation energy is found to be

$E_{a\,(1.5\,kbar)}$ = 2.6 kcal.mol^{-1} (10.9 kJ.mol^{-1}) (10)

Increasing pressure decreases considerably the energy barrier of the self-cleavage reaction and at the same time the rates of catalysis decrease. Such results indicate that pressure perturbs the different active site structures of the ASBVds leading to a new less active global conformer. The global stability of the RNA's structure is conserved as shown by an identical temperature-inactivation value $T_{inact.}$ = 55°C.

A detailed analysis of the pressure-dependent of the reac-

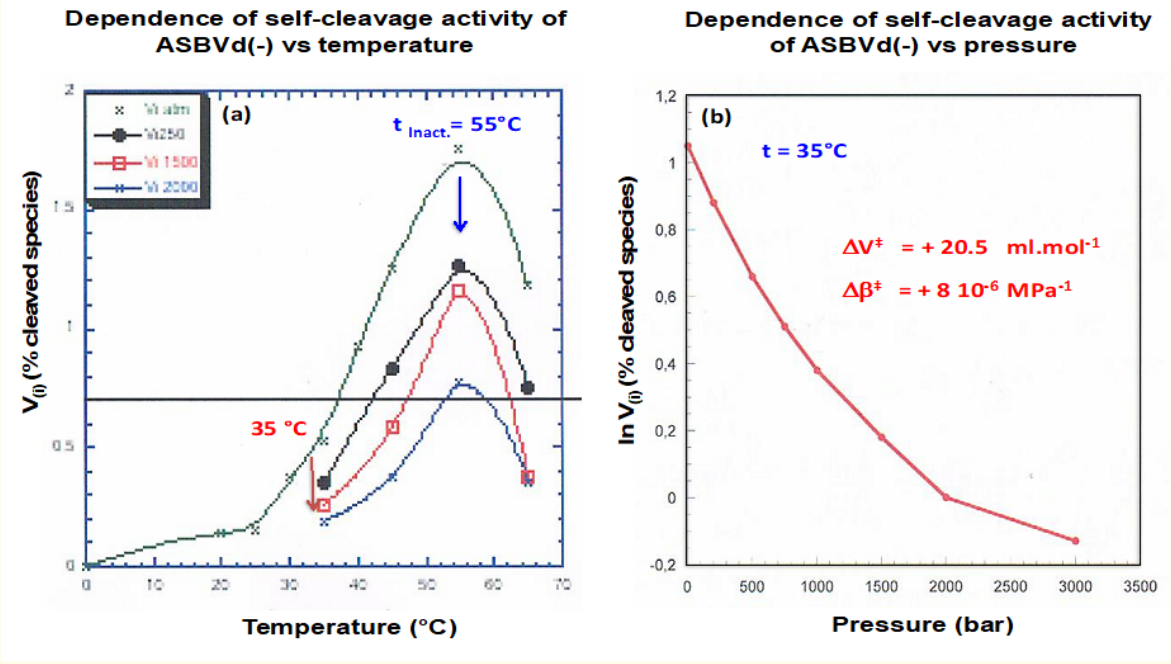

Figure 9: Effects of temperature and high pressure on the kinetic behavior of ASBVd(-) self-cleavage activity. Panel **(a)** shows the temperature profile of the rates as a function of high pressure. Curve green is at 1 bar, curve black at 1.25 kbar, curve red at 1.5 kbar and curve blue at 2.5 kbar. The horizontal black line is referred to an activity giving 75% cleaved species. Panel **(b)** shows the multiphasic behavior of the self-cleaved kinetic of ASBVd(-) at 35°C versus high pressure (red curve). (red curve). A quadratic curve fitting of the acitivity curve of ASBVd(-) gives an activation volume of + 20.5 ml mol^{-1} and an activation isothermal compressibility equal to 8 10^{-6} MPa^{-1}.

tion rates is shown in **Figure 9 (b)**, where at 35°C and 1.5 kbar, a complex pressure-induced multiphasic kinetic behavior is found. Pressure-induced inactivation of the observed rate of ASBVd(-) viroid is a non-linear decay curve. Following equation (4), we can extract an activation volume and an activation isothermal compressibility of the self-cleavage process to be

$\Delta V^{\ddagger} = + 20.5$ ml.mol^{-1} .....(11)

$\Delta\beta^{\ddagger} = + 8\ 10^{-6}$ MPa^{-1}

These results indicate that the self-cleavage active site of ASBVd(-) is controlled by a complex global conformational flexible folding. Pressure acts as a reversible unfolding effect in the global structure around the HHD site leading to a less active conformers. The activation volume and the isothermal compressibility are quite important. The positive value of $\Delta\beta^{\ddagger}$ indicate that the viroid is compressible presumably associated with compression of cavities in the interior of ASBVd(-) or changes in intermolecular packing.

Interestingly, to overcome such structural complexity behaviour, Kaddour H., *et al*. had undertaken a study of the pressure effect on a ribosyme hammerhead from the *chrysanthemum* chlorotic mottle viroid wherein the structure is simpler [54]. Their results show that a biphasic profile of the cleavage reaction is observed at 1 bar. The analysis gives 2 well-fitted exponential components, such a fast rate $k_{fast.}$ (4.9 10^{-2} min^{-1}) and a slow rate $k_{slow.}$ (2.5 10^{-3} min^{-1}). An increase of pressure perturbs differently the profile of the two rates, leading to 2 positive activation volumes equal to $\Delta V^{\ddagger}_{fast.}$ = 2.6 ml.mol^{-1} and $\Delta V^{\ddagger}_{slow.}$ = 11.5 ml.mol^{-1}. It is interpreted as, during the self-cleavage reaction the hammerhead ribozyme undergoes some more simple conformational changes than in the case of ASBVd(-) viroid. The « fast populations » represent molecules in the near-active site's conformation, whereas « slow populations » represent molecules that need a larger change in conformation to induce activity.

Conclusion and Perspectives

In the present study, we have developed a combined use of NIR Raman spectroscopy technique and a baro bio-reactor to probe the structure and activity of RNA from *Avocado Sunblotch* viroids (ASBVd) in response to changes in the extreme environmental conditions. NIR Raman spectroscopy is an interesting technique for the characterization of the vibrational modes of RNA molecule to establish a reliable correlation between Raman vibrational markers and the specific structural features of RNA and their biological important complexes. It has been shown that the analysis of such Raman markers allows not only to estimate secondary structure, base-base interactions but also tertiary structure of RNA such as sugar pucker structures and bases rotation geometries. It is shown that Raman structural markers are very sensitive to RNA's folding and self-cleavage transesterification process. The typical « A-type » RNA conformation with ordered double helical content and a C3'-endo/anti sugar pucker configuration is destabilized by high temperature leading to loss of base-stacking and loss of « A-type » secondary structure and the appearance of a new nucleotide conformation. D_2O cosolute not only decreases RNA's transesterification kinetics as a consequence of hydrogen-deuterium atom's exchanges, but perturbs the internal loops and base-base interactions leading to a new rearrangement of the helical structure. Interestingly, self-cleavage of the RNA through transesterification process, induces huge frequency downshifts of all the characteristic vibrational modes with little perturbation of their intensities. These vibrational energy decreases are indicative of a cleavage of RNA' structure leading to phosphodiester and phosphodioxy structural changes. The new designed bio-reactor allows to rapidly sampling-out products of reaction at constant pressure, which is maintained by a programmable remote-controlled motor. Gel electrophoresis analysis of the cleaved RNA shows a bell-shape temperature profiles at several high pressure. The found inactivation temperatures are independent of the pressure, however high pressure induces new less active global conformers with identical stabilities. In addition pressure decreases the transesterification reaction rates in a non-linear manner showing that the kinetics of the process is multiphasic and the RNA molecule is compressible. To overcome the structural complexity of the RNA from *Avocado Sunblotch* viroids, it is interesting to compare these results to the activity of a simpler structural model such as a ribozyme hammerhead from *Chrysanthemum* clorotic viroid [54]. Pressure affects the self-cleavage kinetics of such ribozyme in a simple and resolved biphasic phases, indicating the participation of a fast cleaving and a slow cleaving conformers. Clearly the complex and flexible structure of the *Avocado Sunblotch* viroid controls its HHA active center in a manner to prevent the study of mechanical constraint on the active site alone. The present work is the prologue to encourage future studies on the interactions of ASBVds with therapeutic agents and membranes and on the effects of crowder agents on the folding mechanism to obtain conditions for a « dock structure » of the RNA from both *Avocado Sunblotch* viroids.

Acknowledgement

We thank Jacques Verne and Hussein Kaddour for plasmid's construction and purification of the ASBVds viroids. Hussein Kaddour who was recipient of fellowship from the Center National de la Recherche Scientifique (CNRS, FRANCE) had doing most of the Raman experiments. Vanina Mahadeo a student from CNRS,

Hussein Kaddour and Hervé Guy from UPMC Univ. Pierre et Marie Curie, Paris, France, are gratefully acknowledged for activity measurements of ASBVd under high pressure. This study was supported by University Paris 6, the CNRS (grant PID EPOV) and the Centre National d'Etudes Spatiales. We thank Philippe Chopineau from Top Industrie (France) for the design and construction of the high pressure bio-reactor. BMC Biophysics (BioMed Center) [37] is thank for the reproductions of some Figures.

Authors's Contributions

GHBH, SGK and MCM conceptualized the study and wrote the manuscript. HK and JV have performed the purification of the viroids. HK and SGK have doing Raman experiments while SGK and PCh have setup respectively the Raman instrumentation and the high pressure bio-ractor. SGK and GHBH performed Raman data treatment and GHBH the analysis of ASBVd's self-cleavage kinetics versus temperature and pressure. VM, HD and HG have performed the self-cleavage activity meausurments. All authors approved the final manuscript.

Bibliography

1. Zhou H-X., *et al.* "Macromolecular crowding and confinement: biochemical, biophysical, and potential physiological consequences". *Annual Review of Biophysics* 37 (2008): 375-397.

2. Zimmerman SB and Trach SO. "Estimation of macromolecule concentrations and excluded Volume effects for the cytoplasm of Escherichia coli". *Journal of Molecular Biology* 222.3 (1991): 599-620.

3. Ellis RJ. "Macromolecular crowding: an important but neglected aspect of the intracell environment". *Current Opinion in Structural Biology* 11 (2001):114-119.

4. Minton AP. "The influence of macromolecular crowding and macromolecular confinement on biochemical reactions in physiologicalmedia". *Journal of Biological Chemistry* 276 (2001): 10577-10580.

5. Yoshikawa K., *et al.* "Compaction of DNA induced by like-charge protein: opposite salt-effect against the polymer-salt-induced condensation with neutral polymer". *The Journal of Physical Chemistry Letters* 1 (2010): 1763-1766.

6. Xue Y., *et al.* "Human Telomeric forms parallel-stranded intramolecular G-Quadruplex in K+ solution under molecular crowding condition". *Journal of the American Chemical Society* 129.36 (2007): 11185-11191.

7. Heddi B and Phan AT. "Structure of human Telomeric DNA in crowded solution". *Journal of the American Chemical Society* 133 (2011): 9824-9833.

8. Bloomfield VA. "DNA condensation". *Current Opinion in Structural Biology* 6.3 (1996): 334-341.

9. S-i N and Sugimoto N. "Model studies of the effects of intracellular crowding on nucleic acid interactions". *Molecular BioSystems* 13 (2017): 32-41.

10. Barron LD., *et al.* "Raman optical activity comes of age". *Molecular Physics* 102 (2004): 731-744.

11. Fanconi B., *et al.* "Polarized laser Raman studies of biological polymers". *The Journal of Chemical Physics* 51 (1969): 3993-4005.

12. Wartell RM and Harrell JT. "Characteristics and variations of B-type DNA conformations in solution - a quantitative analysis of Raman band intensities of 8 DNAs". *Biochemistry* 25 (1986): 2664-2671.

13. Small EW and Peticolas WL. "Conformational dependence of Raman scattering intensities from polynucleotides. 3. Order-disorder changes in helical structures". *Biopolymers* 10.8 (1971): 1377-1416.

14. Erfurth SC., *et al.* "Determination of backbone structure of nucleic acids and nucleic-acid oligomers by laser Raman scattering". *Proceedings of the National Academy of Sciences of the United States of America* 69.4 (1972):938-941.

15. Tsuboi M., *et al.* "Raman Tensors and their application in structural studies of biological systems". *Proceedings of the Japan Academy, Ser. B, Physical* 85 (2009): 83-97.

16. Meersman F., *et al.* "On the Thermal Expansion of Water and the Phase Behavior of Macromolecules in Aqueous Solution". *Chemical Society Reviews* 35 (2006): 908-917.

17. Weber G and Drickramer HG. "The effect of high pressure upon proteins and other biomolecules". *Quarterly Reviews of Biophysics* 16 (1983): 89-112.

18. Jaenicke R. "Biochemical processes under high hydrostatic pressure". *Naturwissenschaften* 70 (1983): 332-341.

19. Heremens K. "High pressure effects on proteins and other biomolecules". *Annual Review of Biophysics and Bioengineering* 11 (1982):1-21.

20. Morild E. "The theory of pressure effects on enzymes". *Advances in Protein Chemistry* 34 (1981): 9-166.

21. Hui Bon Hoa G., *et al.* "A reactor permitting injection and sampling for steady state studies of enzymatic reactions at high pressure: tests with aspartate transcarbamylase". *Analytical Biochemistry* 187 (1990): 258-261.

22. Rocheleau L and Pelchat M. "The Subviral RNA Database: a toolbox for viroids, the hepatitis delta virus and satellite. RNAs research". *BMC. Microbiology* 6 (2006): 6-24.

23. Daros JA and Flores R. "Arabidopsis thaliana has the enzymatic machinery for replicating representative viroid species of the family Pospiviroidae". *Proceedings of the National Academy of Sciences of the United States of America* 101.17 (2004): 6792-6797.

24. Khvorova A., *et al.* "Sequence elements outside the hammerhead ribozyme catalytic core enable intracellular activity". *Nature Structural and Molecular Biology* 10.9 (2003): 708-712.

25. Chen J-H., *et al.* "A 1.9 angstrom Crystal Structure of the HDV Ribozyme precleavage suggests both Lewis acid and general acid mechanisms contribute to phosphodiester cleavage". *Biochemistry* 49.31 (2010): 6508-6518.

26. Daros JA., *et al.* "Replication of avocado sunblotch viroid evidence for a symmetrical pathway with 2 rolling circles and hammerhead ribozyme processing". *Proceedings of the National Academy of Sciences of the United States of America* 91.26 (1994): 12813-12817.

27. Gora-Sochacka A. "Viroids: unusual small pathogenic RNAs". *Acta Biochimica Polonica* 51.3 (2004): 587 607.

28. Wild U., *et al.* "Loops in viroids - accessibility to transfer RNA anticodon binding". *European Journal of Biochemistry* 103 (1980):227-235.

29. Ding B and Itaya A. "Viroid: A useful model for studying the basic principles of infection and RNA biology". *Molecular Plant-Microbe Interactions* 20.1 (2007):7-20.

30. Gong B., *et al.* "Competition between Co (NH (3)) (6) (3+) and inner sphere Mg (2+) ions in the HDV ribozyme". *Biochemistry* 48.50 (2009):11961-11970.

31. Mozhaev VV., *et al.* "High pressure effects on protein structure and function". *Biochemistry and Molecular Biology International* 24 (1996): 81-91.

32. Royer C and Winter R. "Protein hydration and volumetric properties". *Current Opinion in Colloid and Interface Science* 16 (2011): 568-571.

33. Rouget JB., *et al.* "Size and sequence and the volume of protein folding". *Journal of the American Chemical Society* 133 (2011): 6020-6027.

34. Masson P and Balny C. "Linear and non-linear pressure dependence of enzyme, catalytic parameters". *Biochimica et Biophysica Acta* 1724 (2005): 440-450.

35. Truhlar DG., *et al.* "Current Status of Transition-State Theory". *The Journal of Physical Chemistry* 100 31 (1996):12771-12800.

36. Kovermann M., *et al.* "Structural basis for catalytically restrictive dynamics of high-energy enzyme state". *Nature Communications* 6 (2015): 7644-7674.

37. Hui Bon Hoa G., *et al.* "Raman characterization of Avocado Sunblotch viroid and its response to external perturbations and self-cleavage". *BMC Bipphysics* 7.1 (2014): 2-15.

38. Tsuboi M., *et al.* "Raman spectrum of a transfer RNA". *Science* 174.4014 (1971): 1142-1144.

39. Chen Y., *et al.* "Probing adenine rings and backbone linkages using base specific isotope-edited Raman spectroscopy: application to group II intron ribozyme domain V". *Biochemistry* 49.16 (2010): 3427-3435.

40. Hartman KA., *et al.* "Studies of virus structure by laser Raman spectroscopy. 4. Turnip yellow mosaic-virus and capsids". *Biochemistry* 17 (1978): 2118-2123.

41. Hernandez B., *et al.* "Thermodynamic and structural features of ultrastable DNA and RNA hairpins". *Journal of Molecular Structure* 651 (2003): 67-74.

42. Nishimura Y., *et al.* "Raman diagnosis of nucleic-acid structure - sugar puckering and glycosidic conformation in the guano-

sine moiety". *Nucleic Acids Research* 11.5 (1983):1579-1588.

43. Erfurth SC., *et al.* "Determination of backbone structure of nucleic acids and nucleic-acid oligomers by laser Raman scattering". *Proceedings of the National Academy of Sciences of the United States of America* 69 (1972): 938-941.

44. Erfurth SC and Peticolas WL. "Melting and premelting phenomenon in DNA by laser Raman scattering". *Biopolymers* 14 (1975): 247-264.

45. Brown EB and Peticolas WL. "Conformational geometry and vibrational frequencies of nucleic-acid chains". *Biopolymers* 14 (1975): 1259-1271.

46. Thomas GJ., *et al.* "In Biomolecular Stereodynamics, vol. IV. edited by Sarma S, Sarma A. NY. Adenine Press Guilderland (1986): 227.

47. Thomas GJ and Hartman KA. "Raman studies of nucleic acids. 8. Estimation of RNA secondary structure from Raman scattering by phosphate group vibrations". *Biochimica et Biophysica Acta* 312 (1973): 311-322.

48. Benevides JM., *et al.* "Raman studies of nucleic-acids. 41. Design of the helix-turn helix motif - nonlocal effects of quaternary structure in DNA recognition investigated by laser Raman spectroscopy". *Biochemistry* 30.18 (1991): 4381-4388.

49. Nishimura Y and Tsuboi M. "Local conformations and polymorphism of DNA duplexes as revealed by their Raman spectra. In Advances in Spectroscopy, Vol. 13. Spectroscopy of Biological Systems. Edited by Clark RJ, Hester AE. New York: Wiley (1986): 17-232.

50. Medeiros GC and Thomas GJ. "Raman studies of nucleic acids. 4. Vibrational spectra and associative interactions of aqueous inosine derivatives". *Biochimica et Biophysica Acta* 247 (1971): 449-462.

51. Hartman KA., *et al.* "Studies of virus structure by laser Raman spectroscopy. 4. Turnip yellow mosi-virus and capsids". *Biochemistry* 17 (1978): 2118-2123.

52. Valdemaras R. "Interactions of cyclic AMP and its dibutyryl analogue with model membrane: X-ray diffraction and Raman spectroscopy study unsing liquid-crystalline phases of monoolein". *Biophysical Chemistry* 90.1 (2001):75-87.

53. Fujimoto N., *et al.* "Effects of hydrogen bondings on the UV resonance Raman bands of adenine ring and its C8-deuterated analog". *Journal of Molecular Structure* 447 (1998): 61-69.

54. Kaddour H., *et al.* "High-pressure analysis of a hammerhead ribozyme from Chrysanthemum chlorotic mottle viroid reveals two different populations of self-cleaving molecule". *FEBS Journal* 278.19 (2011): 3739-3743.

Volume 2 Issue 9 September 2019